5-2-2022

A Dual-Band Filtering Structure for Highly Selective Reconfigurable Bandpass Filter and Filtering Balun

Jinqun Ge

Guoan Wang
University of South Carolina, gwang@cec.sc.edu

Publication Info

Published in *International Journal of RF and Microwave Computer-Aided Engineering*, Volume 32, Issue 8, 2022.

Received: 2 March 2022 | Revised: 23 April 2022 | Accepted: 25 April 2022

DOI: 10.1002/mmce.23215

ORIGINAL ARTICLE

INTERNATIONAL JOURNAL OF RF AND MICROWAVE COMPUTER-AIDED ENGINEERING WILEY

A dual-band filtering structure for highly selective reconfigurable bandpass filter and filtering balun

Jinqun Ge | **Guoan Wang**

Department of Electrical Engineering, University of South Carolina, Columbia, South Carolina, USA

Correspondence
Guoan Wang, Department of Electrical Engineering, University of South Carolina, Columbia, SC 29208, USA.
Email: gwang@cec.sc.edu

Funding information
National Science Foundation, Grant/Award Number: 1910853

Abstract

This article proposes a filtering structure consisting of two half-wavelength resonators and two open-stub loaded resonators, which generates two third-order passbands. Multiple transmission zeros are introduced by the newly developed coupling scheme, resulting in extremely sharp roll-off desirable for highly selective filters. The proposed structure is applied to design a PIN-diodes switch-controlled reconfigurable dual-band bandpass filter (BPF) with four-state filtering responses: both passbands ON, both passbands OFF, high-frequency passband ON, and low-frequency passband ON. Stepped-impedance open stubs and one-end-grounded coupled lines are studied and employed in the design to suppress unwanted responses. In addition, two filtering structures are placed symmetrically to design a dual-band balun BPF. Double-sided parallel-strip lines are added in the input port of the filter, and their inherent out-of-phase feature enables the balun filter to convert unbalanced signal to balanced signal at desired frequencies. The measured results of both fabricated devices agree well with the simulated results. The switchable BPF and balun BPF have two passbands (2.8 and 4.8 GHz) with high selectivity with the minimum roll-offs from −3 to −15 dB are 1.70×10^3 and 2.71×10^3 dB/decade, respectively. The insertion loss of the switchable BPF is 2.3/2.0 dB and the minimum signal suppressions level OFF state is measured as −18.2 dB. The insertion loss of the balun BPF is 1.8/1.4 dB, and the phase and magnitude imbalances are less than 0.3 dB and 5°, respectively. The excellent performances of the implemented filter and filtering balun successfully demonstrate the advantages and design efficacy of the proposed filtering structure for different applications.

KEYWORDS

balun BPF, dual-band, filtering structure, sharp roll-off, switchable BPF

1 | INTRODUCTION

The vigorous development of communication technologies has laid a solid foundation for various applications such as autonomous driving, smart home appliances, and industrial IoTs. However, current and future wireless communication systems are demanded for technical improvement to support multiple wireless communications bands and protocols. Multiband cognitive radio has been widely considered as one of the prominent solutions

to tackle the spectrum scarcity with significantly enhanced throughput and better channel maintenance of communication networks.[1,2] Multiband and multiple function components such as bandpass filters (BPFs) are of great importance in improving system spectral efficiency, system space-consuming, and multi-function capability.[3] Yet, the rapid development of system integration requires multiple filters to work simultaneously within narrow proximity bands, resulting in great demand of filters with high selectivity to make best use of the limited spectrum resources and to reject the interfering signals.[4]

To meet the ever-increasing requirements of multi-band and multi-function communication systems, BPFs are required to provide good signal selectivity and enhanced functions simultaneously. Figure 1A gives a typical configuration of a front-end module, where balun, switches, power amplifier (PA), low-noise amplifier (LNA) and BPFs are employed to enable multi-channel communications. If the BPF is designed to achieve reconfigurable dual passbands, which provides adaptive filtering response to accommodate changes in the available spectrum, the entire module can be significantly simplified as shown in Figure 1B.[5–10]

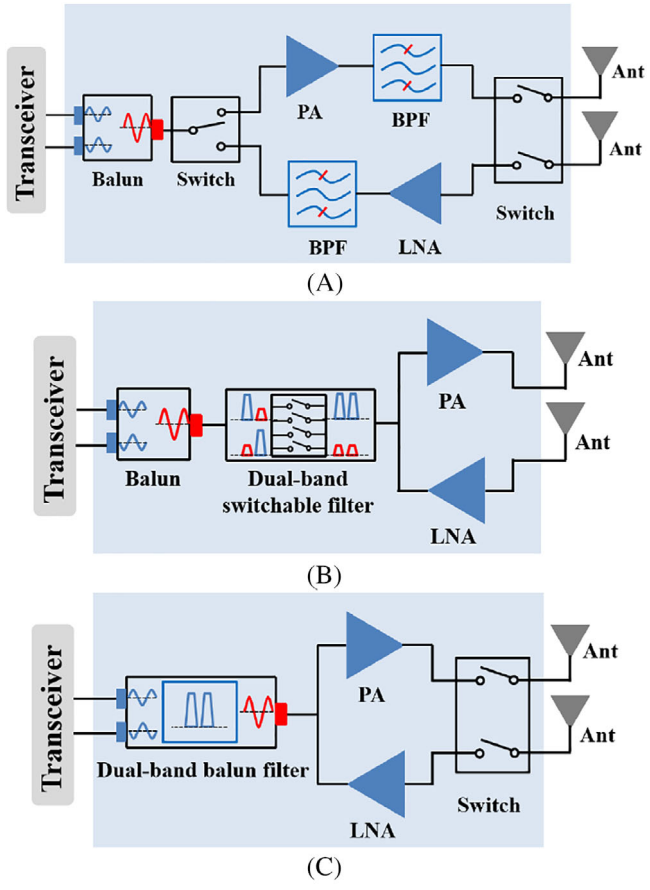

FIGURE 1 (A) Typical configuration of a front-end module. Simplified module enabled with (B) dual-band switchable filter and (C) dual-band balun filter

Technologies, such as combing stub-loaded resonators with transition structures,[7] using dual-frequency resonators[8] or connected-coupling lines[9] and employing stepped-impedance open stubs,[10] and so forth, have been developed to achieve switchable dual-band filtering responses. However, maintaining sharp roll-off, achieving low insertion loss at ON-state, and providing deep signal suppression level at OFF-state, are key technical challenges in designing switchable dual-band BPFs. Similarly, as depicted in Figure 1C, the size and cost of the module are reduced by integrating dual-band BPFs with balun function. Balun filters convert unbalanced signals to balanced signals and provide filtering responses simultaneously. Although filtering balun structures have been widely achieved with microstrip branch lines,[11] substrate integrated waveguides,[12] stub loaded resonators,[13] and dielectric resonators,[14] the integrated technologies for balun function inevitably deteriorate the performance of filters, including poor selectivity and extra insertion loss.[15] Thus, lower loss, smaller size, and higher selectivity are consistent pursuits in the design of multi-functional dual-band BPFs. Nevertheless, high selectivity of dual-band BPFs is hard to achieve with regular filtering structures due to the limited transmission zeros and coupling restrictions. Designing dual-band BPFs with sharp roll-off and good out-of-band rejection remains a challenging task, especially for BPFs with frequency reconfigurability or balun functions.

In this article, a novel filtering structure enabled with half-wavelength resonators and open-stub loaded resonators is presented to provide high-order passbands. By properly designing the coupling scheme, multiple transmission zeros are introduced to achieve extremely high selectivity at passbands. Based on the proposed structure, a PIN-diode-controlled reconfigurable dual-band BPF and a dual-band filtering balun are designed and implemented to demonstrate the design efficacy. In Section 2, the working principles of the basic filtering structure are fully investigated with thorough theoretical analyses. In Section 3, measured results of the PIN-diode controlled reconfigurable BPF are presented. Furthermore, double-sided parallel-strip lines (DSPSL) are integrated into the proposed filtering structure to generate a balanced filtering response, and a filtering balun is implemented with results shown in Section 4. The measured results of the balun filter fully demonstrate the advantages of designing highly selective and multi-functional BPFs with the proposed filtering structure.

2 | BASIC DUAL-BAND FILTERING STRUCTURE

Open-stub loaded resonator is widely utilized in the design of miniaturized filter due to its inherent two resonant modes.[16,17] Two transmission poles are achieved

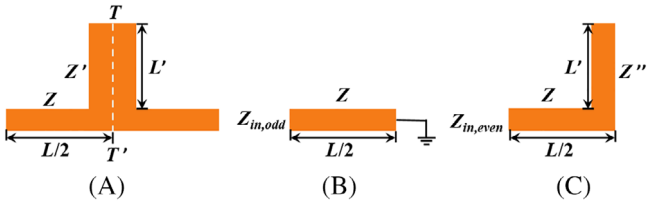

FIGURE 2 (A) Simplified open-stub loaded resonator and its equivalent circuit under (B) odd-mode, and (C) even-mode

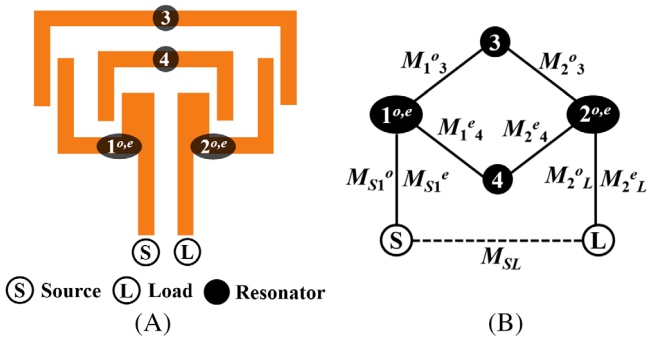

FIGURE 3 (A) Basic dual-band filtering structure and (B) coupling scheme of the filtering structure

with one resonator and their frequencies are highly related to the line length, leading to the controllable performance. To obtain better miniaturization and flexible design, meander line technology is employed in this article to optimize such kind of resonator. As shown in Figure 2A, a simplified open-stub loaded resonator consists of a half-wavelength resonator and an open-stub resonator. The lengths and the characteristic impedances of these two resonators are represented by (L, Z) and (L', Z'), respectively. The two resonant modes of such open-stub resonator are analyzed with the odd–even method. In odd-mode, the resonator is performed as a transmission line ($L/2$) with one-end-grounded and its equivalent circuit is shown in Figure 2B. When the resonance condition of $Y_{in,odd} = 0$ is met, the first odd-mode resonance occurs, and its resonant frequency is:

$$f_{odd} = \frac{c}{2L\sqrt{\varepsilon_{eff}}} \tag{1}$$

where, c is the speed of light in the free space and ε_{eff} is the effective permittivity of the substrate. Obviously, by controlling the L value, the odd-mode resonant frequency can be shifted. On the other hand, in even mode, the resonator's is considered as a half-wavelength resonator with an equivalent circuit illustrated in Figure 2C. When the impedance of the open-stub Z'', whose width is half of the open-stub in Figure 2A, is equal to the impedance of the half-wavelength resonator, that is, $Z = Z''$, the second even-mode resonant frequency is derived as:

$$f_{even} = \frac{c}{(L+2L')\sqrt{\varepsilon_{eff}}} \tag{2}$$

This means that both L and L' affect the even-mode resonant frequency. By changing the length of L and L' separately, independent control of the two transmission poles is realized, which provides a high degree of design freedom for reconfigurable filters.

With the integration of the open-stub loaded resonators and half-wavelength resonators, a miniaturized filtering structure with a third-order dual-band filtering response is achieved. As shown in Figure 3A, two open-stub loaded resonators are placed symmetrically with two half-wavelength resonators and are configured in meander line shape for reduced area. The coupling scheme of this filtering structure is illustrated in Figure 3B, which shows that multiple transmission poles and zeros are introduced. The odd-modes and even-modes of the two open-stub loaded resonators are denoted by 1° and 1^{e}, 2° and 2^{e}, respectively. The two half-wavelength resonators 3 and 4 provide signal propagation path between the two open-stub resonators. In odd-mode, resonators 1°, 2°, and 3 generated three transmission poles to form a low-frequency passband. For even-mode excitation, a high-frequency passband is generated with resonators 1^{e}, 2^{e}, and 4. With the two separate transmission paths of the passbands, the passbands' properties, for example, frequency location, insertion loss, and bandwidth, can be controlled independently. Besides the transmission poles, the source-load coupling between the input and output and the cross-coupling between the resonators within the filtering structure also generate multiple transmission zeros. By carefully locating the transmission poles and zeros, two third-order passbands with sharp roll-off and good out-of-band suppression are eventually realized.

To further characterize the working mechanism of the proposed filtering structure, coupling matrixes [M] are developed to describe the coupling relationships among resonators. Due to the different roles of resonators, the coupling coefficients M_{ij} in the matrix are different under odd-mode and even-mode. Based on the above analysis, the coupling matrixes at odd-mode and even-mode are derived as:

$$[M^{o}] = \begin{bmatrix} 0 & M_{S1^{o}} & 0 & 0 & M_{SL} \\ M_{S1^{o}} & M_{11} & 0 & M_{1^{o}3} & 0 \\ 0 & 0 & M_{22} & M_{2^{o}3} & M_{2^{o}L} \\ 0 & M_{1^{o}3} & M_{2^{o}3} & M_{33} & 0 \\ M_{SL} & 0 & M_{2^{o}L} & 0 & 0 \end{bmatrix} \tag{3}$$

$$[M^e] = \begin{bmatrix} 0 & M_{S1^e} & 0 & 0 & M_{SL} \\ M_{S1^e} & M_{11} & 0 & M_{1^e4} & 0 \\ 0 & 0 & M_{22} & M_{2^e4} & M_{2^eL} \\ 0 & M_{1^e4} & M_{2^e4} & M_{44} & 0 \\ M_{SL} & 0 & M_{2^eL} & 0 & 0 \end{bmatrix} \quad (4)$$

The values of the coupling coefficients M_{ij} are determined by the specific dimensions of the structure. Once the structure is defined, the corresponding coupling matrix can be obtained by fitting the initial guess for the optimization.[18] The loop currents grouped in a 5×5 identity matrix $[I]$ are given as:

$$[-jR + \omega'[W] + [M^{o,e}]][I] = [A][I] = -j[e] \quad (5)$$

where, $j^2 = -1$, $[R]$ is a 5×5 matrix whose only nonzero entries are $R_{11} = R_{55} = 1$, $[W]$ is similar to $[I]$, except that $W_{11} = W_{55} = 0$. The excitation vector is $[e]^t = [1, 0, 0, 0, 0]$. The low-pass prototype frequency ω' is related to the actual frequency ω by $\omega' = \omega_0/\Delta\omega(\omega/\omega_0 - \omega_0/\omega)$, where ω_0 is the center frequency of the filtering circuit and $\Delta\omega$ is its bandwidth. Eventually, the transmission and reflection coefficients of the proposed filtering structure are obtained by (load and source resistors = 1):

$$S_{21} = -2j\left[A^{-1}\right]_{5,1} \quad (6)$$

$$S_{11} = 1 + 2j\left[A^{-1}\right]_{1,1} \quad (7)$$

The determined model can be applied to optimize the design of filter minimizing time-consuming full-wave simulation.

3 | SWITCHABLE DUAL-BAND BPF

Based on the proposed filtering structure, a dual-band BPF is designed by Ansys HFSS with four independently controlled passband states: both passbands ON, both passbands OFF, high-frequency passband ON, and low-frequency passband ON. As shown in Figure 4, the proposed filtering structure in Section 2 is utilized to generate two third-order passbands with high selectivity. Four PIN diodes are employed to control the connections between signal lines and the ground (GND). The diodes D_{L1} and D_{L2} are located at the odd-mode transmission path to control the operating state of the low-frequency passband. Similarly, the diodes D_{H1} and D_{H2} are arranged at the even-mode transmission path to determine the working state of the high-frequency passband. As shown in Table 1, when a group of diodes are turned on, the connected signal suppression mechanism will be activated, resulting in the OFF-state of the corresponding passband.

To achieve better OFF-state rejection, two signal suppression techniques are employed in the switchable filter. As shown in Figure 5A, when one end of a coupled line is grounded, the input signal from port 1 will not pass through the coupled line to the output port 2. This technique is applied to the proposed filter by grounding one end of the signal lines with diodes D_{L2} and D_{H2}. Another signal suppression technique of shunting a stepped-impedance open stub to a transmission path is also applied in this filter, as illustrated in Figure 5B. The introduced stub generates a notch frequency response,

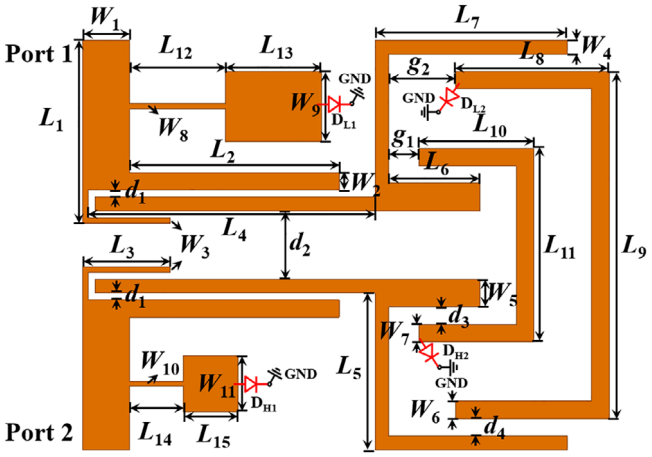

FIGURE 4 Architecture of the switchable dual-band BPF. BPF, bandpass filter

TABLE 1 Four-state filtering responses summary

Activated switches	Filtering states
None	Both bands ON
D_{L1}, D_{L2}, D_{H1}, and D_{H2}	Both bands OFF
D_{H1} and D_{H2}	Low-frequency band ON
D_{L1} and D_{L2}	High-frequency band ON

FIGURE 5 Signal suppression technologies utilized in the filter: (A) one-end-grounded coupled line and (B) stepped-impedance open stub

TABLE 2 Parameter values used in the switchable BPF

Param.	L_1	L_2	L_3	L_4	L_5	L_6	L_7	L_8	L_9	L_{10}
(mm)	10.2	12	5	16	9	5.2	11	8.8	19.9	6.6
L_{11}	L_{12}	L_{13}	L_{14}	L_{15}	W_1	W_2	W_3	W_4	W_5	W_6
11.1	5.5	5.5	3.1	3.1	2.65	1	0.3	0.8	1.6	1
W_7	W_8	W_9	W_{10}	W_{11}	g_1	g_2	d_1	d_2	d_3	d_4
1	0.3	4	0.3	3.2	1	3.8	0.4	3.9	1	1

Abbreviation: BPF, bandpass filter.

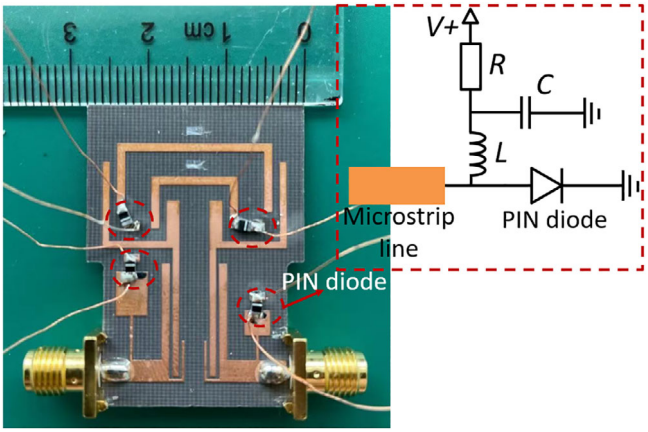

FIGURE 6 Photograph of the fabricated PIN diodes controlled reconfigurable BPF, and biasing circuit of diode (insert). BPF, bandpass filter

thereby enhances the signal suppression. The operating frequency of the notch response is mainly determined by the total length of the open stub while the bandwidth is affected by the ratios of Z_{s1} and Z_{s2}. Moreover, when the open stub is grounded, the influence of the notch response is eliminated. Therefore, two stepped-impedance open stubs are utilized in the proposed filter for each passband, and the working states of the filter are controlled by the diodes D_{L1} and D_{H1}. Eventually, the diodes D_{L1} and D_{L2}, D_{H1} and D_{H2} are used to switch the states of low-frequency band and high-frequency band, respectively.

The optimized switchable dual-band BPF is fabricated on a F4B ($\varepsilon_r = 2.65$, $\tan\delta = 0.0035$) substrate with a thickness of 1 mm. The values of the parameters in Figure 4 are shown in Table 2. Figure 6 shows optical image of a fabricated filter with SMP1322-079 PIN diodes from Skyworks selected as control switches.[19] The insert in Figure 6 also illustrates the biasing circuit for each diode, which is formed with a RF choke inductor $L = 180$ nH, a bypass capacitor $C = 33$ pF, and a resistor $R = 100\ \Omega$, respectively.

The fabricated sample is measured by Rohde & Schwarz ZVA 67, and the results comparisons with four-state filtering responses are depicted in Figure 7A–D. When all the diodes are turned off, an original filter with two third-order passbands is presented in Figure 7A. The center frequencies of the two passbands are measured at 2.85 and 4.86 GHz, respectively. The first passband has a −3 dB bandwidth of 174.

MHz while the −3 dB bandwidth of the second passband is 291 MHz. The minimum insertion losses of the two passbands are 2.3 and 2.0 dB, which are slightly higher than the simulated results. The additional loss is contributed by the loss from PIN diodes and SMA connectors. Multiple transmission zeros contribute to the high selectivity and good out-of-band rejection. The minimum roll-off from −3 to −15 dB is measured as 1.70×10^3 dB/decade and the signal suppression level out of the passbands is better than −20 dB. Instead, when all the diodes are turned on, both passbands will become stopbands due to the activated signal suppression technologies. The filtering response of all frequency blocking is shown in Figure 7B, where signal rejections are better than −18.7 dB. Filtering response of the switchable BPF with only one passband at low frequencies is shown in Figure 7C. The passband at high frequencies is disabled by turning on diodes D_{H1} and D_{H2}, where the maximum rejection level is found as −19.7 dB. Similarly, Figure 7D shows the filtering response with only one passband at high frequencies. Another passband at low frequencies is blocked by turning on diodes D_{L1} and D_{L2} while the minimum rejection level is measured as −18.2 dB.

Table 3 compares the performance of the designed switchable BPF with other similar filters. Most transmission zeros are achieved in the proposed filter, which contributes to the highest selectivity and very good out-of-band suppression. High-order passbands with good miniaturization are realized with multiple meander line resonators in the design. The bandwidth of each band can be increased by slightly separating the transmission poles, which are realizable with different electrical length of the corresponding resonators. In addition, the filter dimension can be further reduced through layout optimization, such as multilayer design.

4 | DUAL-BAND FILTERING BALUN

Compact, efficient, and low-cost signal processing is highly required in modern communication systems.

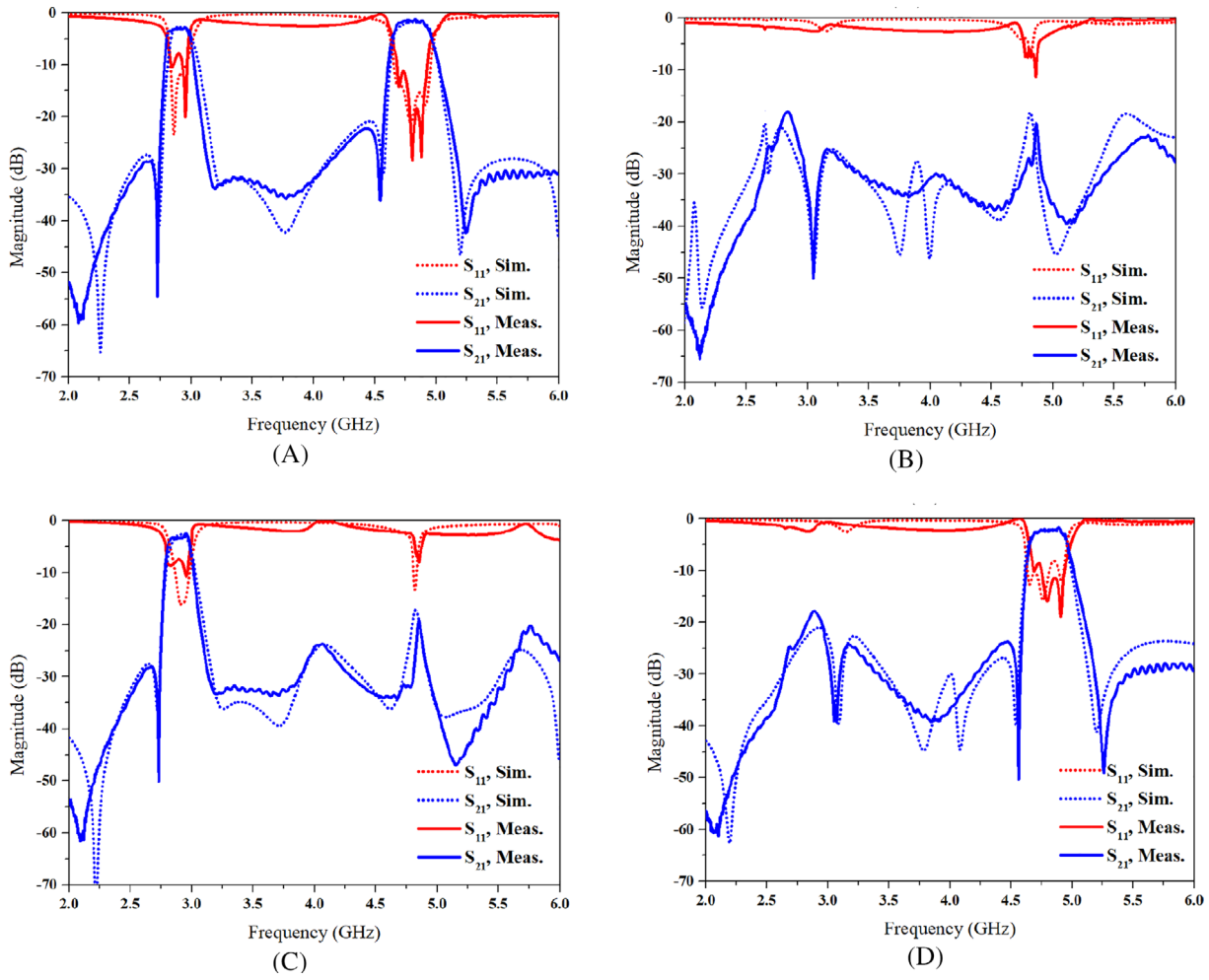

FIGURE 7 Simulated and measured S-parameters of the designed switchable BPF: (A) both passbands ON, (B) both passbands OFF, (C) low-frequency passband ON, and (D) high-frequency passband ON. BPF, bandpass filter

TABLE 3 Comparison with similar references

Refs	f_1/f_2 (GHz)	IL (dB)	TZs	Orders	Selectivity (dB/decade)	Size (λ_g^2)
[6]	1.5/2.0	3.1/3.1	3	3/3	4.2×10^2	0.40
[7]	2.51/3.52	1.2/1.3	5	1/1	6.7×10^2	0.38
[8]	0.9/2.16	2.6/3.2	1	2/2	2.6×10^2	0.17
[9]	1.5/2.5	3.0/2.6	2	2/2	4.0×10^2	0.27
[10]	0.9/2.35	1.4/4.9	0	2/3	5.1×10^2	0.07
Proposed	2.85/4.86	2.3/2.0	6	3/3	17.0×10^2	0.16

Abbreviations: IL, insertion loss; TZs, transmission zeros; λ_g, guided wavelength at the first frequency band.

Baluns are commonly used in these systems to convert the unbalanced signal to the balanced signal between multiple devices, such as filters, amplifiers, antennas, and so forth. The integration of balun and filter can significantly reduce the cost and size of functional blocks, which makes the balun BPF more attractive in recent years. In this section, a dual-band balun BPF based on the presented filtering structure is designed for high selectivity. The symmetrical and planar configuration of the filtering structure makes it suitable for balun design by integrating them back-to-back. As shown in Figure 8, the filtering balun consists of five layers: top resonator, top substrate, middle conductor plane, bottom substrate, and bottom resonator. Two filtering structures are applied on the top and bottom layers to provide dual-band filtering responses. At the input and output of the

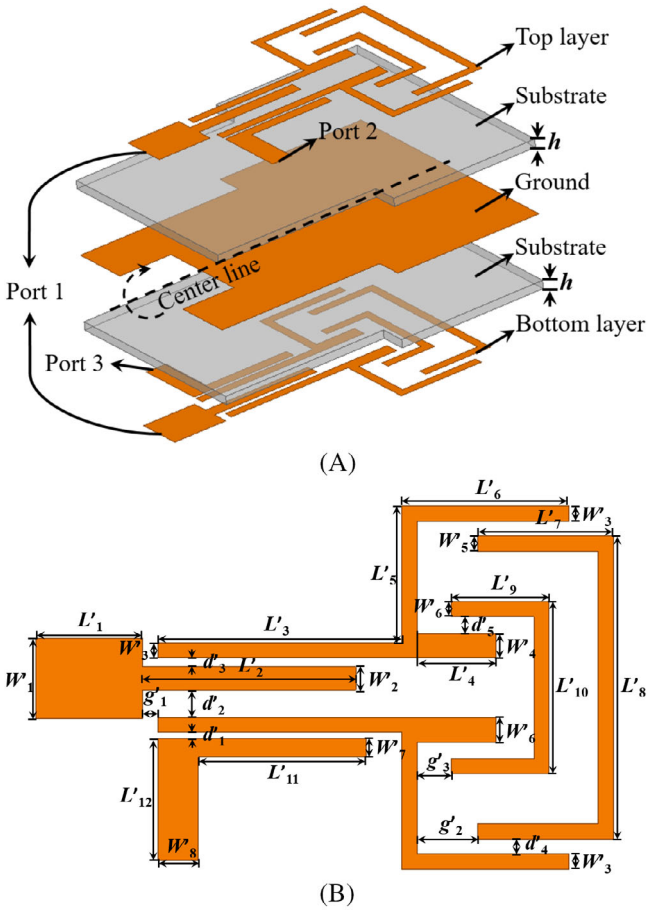

FIGURE 8 (A) 3D view of the dual-band balun BPF. (B) Schematic layout of the top layer. BPF, bandpass filter

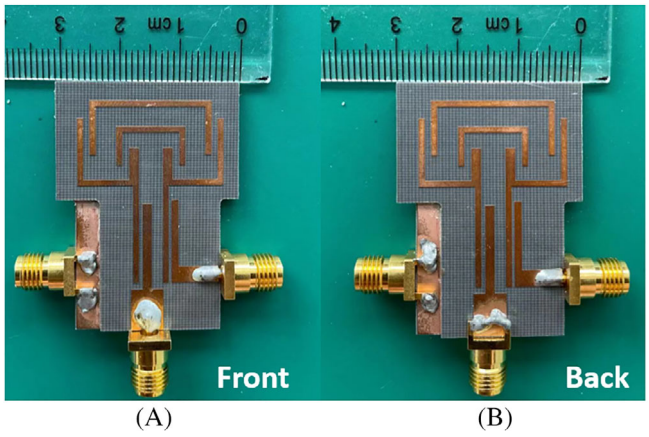

FIGURE 9 Photograph of the fabricated balun BPF: (A) front view and (B) back view. BPF, bandpass filter

filtering structure, two extra metal lines are added for signal diversion. The top layout and the bottom layout are centrosymmetric along the centerline. The conductor plane behaves as a virtual ground for microstrip lines on both sides. It is noted that the ground layer is partially defected, where a DSPSL is formed. The inherent out-of-phase feature of DSPSL makes the filter easy to output balanced signal. Since the filtering structures are excited simultaneously at port 1 on both sides, the input energy is equally separated to port 2 and port 3 with a 180° phase difference.

According to,[20] when the DSPSL has the same width as the converted microstrip line, the characteristic impedance of DSPSL will be twice that of the converted microstrip lines. This property shows great advantages of DSPSL in high impedance applications and enables the easy conversion between the DSPSL and the back-to-back microstrip lines. Eventually, a dual-band balun BPF is constructed to generate a balanced filtering response. The theory in Section 2 is used to analyze and optimize the filtering balun. Since the designed balun BPF consists of two layers of identical filtering structure, the signal at two output ports is half of the calculated results from Equation (6), that is, the calculated transmission coefficients should minus 3 dB for the balun BPF. In addition, the inverse output phases at port 2 and port 3 should be considered during the calculation.

As shown in Figure 9, a well-designed balun BPF is fabricated on F4B ($\varepsilon_r = 2.65$, $\tan\delta = 0.0035$) substrate with dimensions listed in Table 4. The centrosymmetric structure is realized by bonding two identical printed circuit boards (PCBs) with silver glue. In order to soldering SMA conductors to port 2 and port 3, the PCBs are made partially open to expose the intermediated conductor plane without affecting the filter performance.

The simulated and measured results of the balun BPF are presented in Figure 10. Almost the same filtering responses are generated at port 2 and port 3, which fully validate the design efficacy of the proposed balun BPF. The measured center frequencies of the two passbands are 2.89 and 4.81 GHz, respectively. The first passband has a −3 dB bandwidth of 100 MHz while the −3 dB bandwidth of the second passband is 180 MHz. Extremely high selectivity of the two passbands is achieved by the proposed coupling scheme and the minimum roll off from −3 to −15 dB is 2.71×10^3 dB/decade. The minimum insertion losses at two passbands are measured to be (1.77 + 3) and (1.41 + 3) dB. The additional +3 dB in the insertion losses is because the input power is equally divided into the two output ports. The extra loss compared to the simulated results is mainly caused by the manufacturing variation from silver gluing and SMA connectors losses. In addition, the measured transmission zeros are slightly shifted from the simulated *S*-parameters, which are generated by the alignment errors during the bonding process and the use of thicker intermediate conductor plane. To further show the balanced filtering response of the proposed balun BPF, Figure 10B

Param.	L'_1	L'_2	L'_3	L'_4	L'_5	L'_6	L'_7	L'_8	L'_9
(mm)	7	14	16	5.2	9	11	8.9	19.9	6.4
L'_{10}	L'_{11}	L'_{12}	W'_1	W'_2	W'_3	W'_4	W'_5	W'_6	W'_7
11.3	11	8	5.3	1.5	0.8	1.6	1	1	1.2
W'_8	g'_1	g'_2	g'_3	d'_1	d'_2	d'_3	d'_4	d'_5	h
2.65	1	4	2.3	0.4	1.8	0.6	1	1.1	1

TABLE 4 Parameter values used in the filtering balun

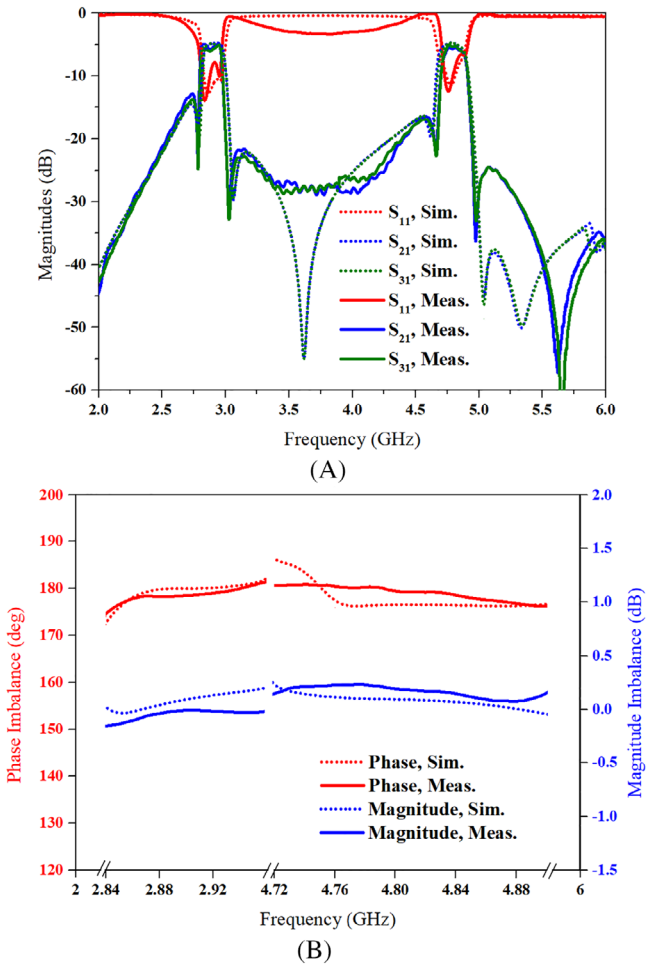

FIGURE 10 Simulated and measured results of the balun BPF: (A) S-parameters and (B) phase and magnitude imbalances of each passband. BPF, bandpass filter

gives the phase and magnitude imbalances of each passband. The maximum imbalances of phase and magnitude are measured as 0.3 dB and 5°, respectively.

Table 5 summarizes the performance comparison of the balun BPF with other similar filters. Due to the additional transmission zeros introduced by the novel coupling scheme, high selectivity and excellent out-of-band rejection are achieved. Adoption of multiple resonators and proper design make the designed balun BPF has high-order passbands and good miniaturization factor. As described in the design of the switchable BPF in Section 3, the bandwidth of the two passbands for the presented filtering balun can be further increased by slightly separating the transmission poles.

5 | CONCLUSION

A novel highly selective filtering structure with a carefully designed coupling scheme is presented in this article. Multiple transmission poles are introduced to form two third-order passbands with half-wavelength resonators and open-stub loaded resonators. Through the proposed coupling scheme, multiple transmission zeros are generated to increase the selectivity of the two passbands. A dual-band BPF with reconfigurable frequency band response and a dual-band balun filter are designed and implemented with the proposed filtering structure. Both devices are measured to be highly selective, with the minimum roll-offs of 1.70×10^3 and 2.71×10^3 dB/decade from -3 to -15 dB, respectively. The good performance of the implemented BPF and filtering balun fully

Refs	f_1/f_2 (GHz)	IL (dB)	FBW (%)	Selectivity (dB/decade)	Size (λ_g^2)
[11]	2.85/3.15	1.9/1.7	5.2/5.1	1.9×10^2	1.95
[12]	9.51/15.0	2.8/2.4	2.7/5.2	19.7×10^2	0.96
[13]	2.44/3.50	2.1/2.2	4.9/2.7	3.6×10^2	0.09
[14]	1.52/1.64	0.9/0.9	0.8/0.9	14.0×10^2	1.56
[15]	3.93/4.14	0.5/0.7	1.0/1.1	22.7×10^3	0.32
Proposed	2.89/4.81	1.8/1.4	3.5/3.7	27.1×10^2	0.18

Abbreviations: IL, insertion loss; λ_g, guided wavelength at the first frequency band.

TABLE 5 Comparison with similar references

demonstrate the design efficacy of the proposed filtering structure for reconfigurable and multifunctional BPFs with high selectivity.

ACKNOWLEDGMENT

The authors would like to thank the funding support from the National Science Foundation under grant 1910853 and software support from ANSYS corporation.

DATA AVAILABILITY STATEMENT

The data that support the findings of this study are available from the corresponding author upon reasonable request.

ORCID

Jinqun Ge https://orcid.org/0000-0003-3440-1964

REFERENCES

1. Mahmoud HHH, Amer AA, Ismail T. 6G: a comprehensive survey on technologies, applications, challenges, and research problems. *Trans Emerg Telecommun Technol*. 2021;32(4):e4233.
2. Wu Y, Fourn E, Besnier P, Quendo C. Direct synthesis of multiband bandpass filters with generalized frequency transformation methods. *IEEE Trans Microw Theory Tech*. 2021;69(8):3820-3831.
3. Zhang Y, Wu Y, Yan J, Wang W. Wideband high-selectivity filtering all-frequency absorptive power divider with deep out-of-band suppression. *IEEE Trans Plasma Sci*. 2021;49(7):2099-2106.
4. Nosrati M, Rezaei P. Compact tunable tri-band bandpass filter using varactor diodes for wireless fidelity, wireless local area network, and worldwide interoperability for microwaves access applications. *Int J RF Microw Comput-Aided Eng*. 2022;32(1):e22935.
5. Ge J, Wang G. Switchable dual-band bandpass filter with high selectivity. In: 2021 IEEE MTT-S International Wireless Symposium (IWS); 2021:1-3.
6. Deng P, Jheng J. A switched reconfigurable high-isolation dual-band bandpass filter. *IEEE Microw Wireless Compon Lett*. 2011;21(2):71-73.
7. Wei F, Zhang CY, Zeng C, Shi XW. A reconfigurable balanced dual-band bandpass filter with constant absolute bandwidth and high selectivity. *IEEE Trans Microw Theory Tech*. 2021;69(9):4029-4040.
8. Tu W-H. Design of switchable dual-band bandpass filters with four states. *IET Microw Antennas Propagat*. 2010;4(12):2234-2239.
9. Chao S, Kuo C, Lin W, Li W, Deng P. A dual-band switchable bandpass filter using connected-coupling mechanisms. In: 44th European Microwave Conference; 2014:941-944.
10. Chuang M, Wu M. Switchable dual-band filter with common quarter-wavelength resonators. *IEEE Trans Circ Syst II: Express Briefs*. 2015;62(4):347-351.
11. Gómez-García R, Munoz-Ferreras J-M, Psychogiou D. Balanced symmetrical quasi-reflectionless single and dual-band bandpass planar filters. *IEEE Microw Wireless Compon Lett*. 2018;28(9):798-800.
12. Zhou K, Kang W, Wu W. Compact dual-band balanced bandpass filter based on double-layer SIW structure. *Electron Lett*. 2016;52(18):1537-1539.
13. Wei F, Yu JH, Zhang CY, Zeng C, Shi XW. Compact balanced dual-band BPFs based on short and open stub loaded resonators with wide common-mode suppression. *IEEE Trans Circ Syst II: Express Briefs*. 2020;67(12):3043-3047.
14. Chen J, Yuan X, Li J, Qin W. Dual-band filtering Balun based on dual-mode dielectric resonator. In: 2018 IEEE International Conference on Computational Electromagnetics (ICCEM); 2018:1-2.
15. Li YC, Li LW, Wu DS, Fang X, Xue Q. Dual-mode dual-band DR Balun filter using suspended Stripline feeding structure. *IEEE Microw Wireless Compon Lett*. 2022;1-4. https://doi.org/10.1109/LMWC.2022.3142906
16. Jiang W, Huang Y, Wang T, Peng Y, Wang G. Microstrip balanced quad-channel diplexer using dual-open/short-stub loaded resonator. In: IEEE MTT-S Int Microw Symp (IMS); 2016:1-3.
17. Jiang W, Shen W, Wang T, Huang Y, Peng Y, Wang G. Compact dual-band filter using open/short stub loaded stepped impedance resonators (OSLSIRs/SSLSIRs). *IEEE Microw Wireless Compon Lett*. 2016;26(9):672-674.
18. Amari S, Rosenberg U, Bornemann J. Adaptive synthesis and design of resonator filters with source/load-multi-resonator coupling. *IEEE Trans Microw Theory Tech*. 2002;50:1969-1978.
19. SMP1322-079LF Skyworks Solutions, Inc. Diode-PIN | Skyworks; 2022. https://store.skyworksinc.com/products/detail/smp1322079lf-skyworks-solutions-inc/259214/
20. Cai J, Yang Y, Qin W, Chen J. Wideband tunable differential bandstop filter based on double-sided parallel-strip line. *IEEE Trans Compon Pack Manuf Tech*. 2018;8(10):1815-1822.

How to cite this article: Ge J, Wang G. A dual-band filtering structure for highly selective reconfigurable bandpass filter and filtering balun. *Int J RF Microw Comput Aided Eng*. 2022;32(8):e23215. doi:10.1002/mmce.23215